The Meteoritical Society

Meteoritics & Planetary Science 45, Nr 1, 7–20 (2010)
doi:10.1111/j.1945-5100.2009.01010.x

Vapor-condensed phase processes in the early solar system

Lawrence GROSSMAN*

Department of the Geophysical Sciences and Enrico Fermi Institute, The University of Chicago, 5734 South Ellis Avenue, Chicago, Illinois 60637, USA
*Corresponding author. E-mail: yosi@uchicago.edu

(*Received 4 August 2009; revision accepted 26 September 2009*)

Abstract–Equilibrium thermodynamic calculations of the sequence of condensation of phases from a cooling gas of solar composition at total pressures thought to have prevailed in the inner part of the solar nebula successfully predict the primary mineral assemblages of refractory inclusions in CM2 and CV3 chondrites. Many refractory inclusions in CM2 chondrites contain a relatively SiO_2-poor assemblage (spinel, hibonite, grossite, perovskite, corundum) that represents a high-temperature stage of condensation, and some may be pristine condensates that escaped later melting. Compact Type A and Type B refractory inclusions, consisting of spinel, melilite, perovskite, Ca-rich clinopyroxene ± anorthite, in CV3 chondrites are more SiO_2-rich and equilibrated with the solar nebular gas at a slightly lower temperature. Textures of many of these objects indicate that they underwent melting after condensation, crystallizing into the same phase assemblage as their precursors. The Ti^{3+}/Ti^{4+} ratio of their pyroxene indicates that this process occurred in a gas whose oxygen fugacity (f_{O_2}) was approximately 8.5 log units below that of the iron-wüstite buffer, making them the only objects in chondrites known to have formed in a system whose composition was close to that of the sun. Relative to CI chondrites, these inclusions are uniformly enriched in a group of elements (e.g., Ca, REE, Zr, Ta, Ir) that are chemically diverse except for their high condensation temperatures in a system of solar composition. The enrichment factor, 17.5, can be interpreted to mean that these objects represent either the first 5.7 wt% of the condensable matter to condense during nebular cooling or the residue after vaporization of 94.3% of a CI chondrite precursor. The Mg and Si isotopic compositions of Types A and B inclusions are mass-fractionated by up to 10 and 4 ‰/amu, respectively. When interpreted in terms of Rayleigh fractionation during evaporation of Mg and Si from the inclusions while they were molten, the isotopic compositions imply that up to 60% of the Mg and up to 25% of the Si were evaporated, and that approximately 80% of the enrichment in refractory ($CaO + Al_2O_3$) relative to more volatile ($MgO + SiO_2$) in the average inclusion is due to initial condensation and approximately 20% due to subsequent evaporation. The mineralogical composition, including the Ti^{3+}/Ti^{4+} ratio of the pyroxene, in Inti, a particle sampled from Comet Wild 2 by the Stardust spacecraft, is nearly identical to that of a Type B inclusion, indicating that comets contain not only the lowest-temperature condensates in the form of ices but the highest-temperature condensates as well. The FeO/(FeO + MgO) ratios of olivine and pyroxene in the matrix and chondrules of carbonaceous and ordinary chondrites are too high to be made in a system of solar composition, requiring f_{O_2}s only 1 or 2 log units below iron-wüstite, more than 10^5 times higher than that of a solar gas. Various ways have been devised to generate cosmic gases sufficiently oxidizing to stabilize significant FeO in olivine at temperatures above those where Fe-Mg interdiffusion in olivine ceases. One is by vertical settling of dust toward the nebular midplane, enriching a region in dust relative to gas. Because dust is enriched in oxygen compared to carbon and hydrogen relative to solar composition, a higher f_{O_2} results from total vaporization of the region, but the factor by which theoretical models have so far

© The Meteoritical Society, 2010. Printed in USA.

enriched the dust is 10 times too low. Another is by transporting icy bodies from the outer part of the nebula into the hot, inner part where vaporization of water ice occurs. Not only does this method fail to make the needed f_{O_2} by a factor of 30–1000 but it also ignores simultaneous evaporation of carbon-bearing ices that would make the f_{O_2} even lower.

Some of the important minerals in this paper are defined by their chemical formulae on Table 1. All contain Ca or Al. Corundum is pure alumina. Two different Ca-, Al-oxides, hibonite and grossite, differ only in their ratios of Al to Ca. Perovskite is Ca-, Ti-oxide. Spinel in the context of this paper is pure Mg-, Al-oxide. Anorthite is a Ca-, Al-silicate. There are two important solid solution minerals. One is melilite, in which åkermanite, a Ca-, Mg-silicate, and gehlenite, a Ca-, Al-silicate, are dissolved in the same crystal structure. The other is fassaite, a Ca-rich clinopyroxene containing four components. One, diopside, contains Mg; one, now called kushiroite, contains Al; one, now called grossmanite, contains Ti^{3+} and one contains Ti^{4+}.

Starting with a gas having the composition of the solar system and a total pressure that might have prevailed in the inner part of the solar nebula, we use thermodynamic calculations to predict the sequence of condensation of minerals while the gas cools (Grossman 1972, 1980; Yoneda and Grossman 1995; Ebel and Grossman 2000). In Fig. 1, results are shown in terms of how Al is distributed between gaseous and crystalline phases as a function of temperature. The first major phase predicted to condense is corundum at about 1730 K. It then reacts with gaseous Ca to form hibonite, CA_6 in Fig. 1, that consumes the corundum. By 1650 K, almost all of the Al is condensed. With falling temperature, more and more gaseous Ca condenses by reacting with pre-existing solids, forming a series of calcium aluminates with declining Al/Ca ratios, from hibonite to grossite (CA_2) to calcium monaluminate (CA). This series reverses below 1575 K as more and more gaseous Si reacts with the condensate to form melilite, progressively removing Ca relative to Al from the residual oxides. Excess hibonite reacts with gaseous Mg to form spinel at about 1470 K. Melilite reacts with the gas to form a fassaitic clinopyroxene at about 1430 K, and then spinel reacts with aluminous pyroxene to form anorthite at about 1375 K.

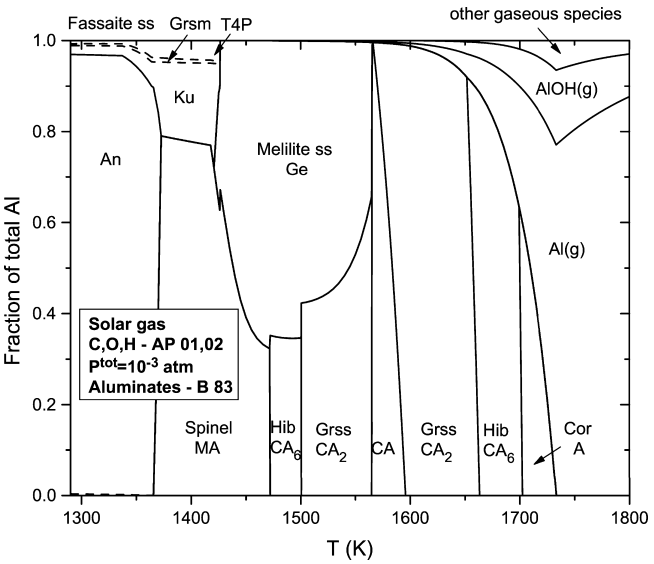

Fig. 1. Equilibrium distribution of Al between vapor and condensed phases in a system of solar composition at a total pressure of 10^{-3} atm, calculated using thermodynamic data for calcium aluminates from Berman (1983) and solar system abundances of carbon and oxygen relative to hydrogen from Allende Prieto et al. (2001, 2002). Dashed curves separate components of solid solutions from one another. Abbreviations: Cor, corundum; A, Al_2O_3; Hib, hibonite; CA_6, $CaO{\cdot}6Al_2O_3$; Grss, grossite; CA_2, $CaO{\cdot}2Al_2O_3$; CA, $CaO{\cdot}Al_2O_3$; Ge, gehlenite; MA, $MgO{\cdot}Al_2O_3$; Ku, kushiroite; Grsm, grossmanite; An, anorthite; ss, solid solution.

Table 1. Important minerals.

		Melilite	
Corundum	Al_2O_3	Gehlenite	$Ca_2Al_2SiO_7$
Hibonite	$CaAl_{12}O_{19}$	Åkermanite	$Ca_2MgSi_2O_7$
		Fassaite	
Grossite	$CaAl_4O_7$	Diopside	$CaMgSi_2O_6$
Perovskite	$CaTiO_3$	Kushiroite	$CaAl_2SiO_6$
Spinel	$MgAl_2O_4$	Grossmanite	$CaTiAlSiO_6$
Anorthite	$CaAl_2Si_2O_8$	T4Px	$CaAl_2TiO_6$

Figure 2 shows how Ca behaves while all those reactions are taking place. After hibonite condenses but before melilite forms, all the Ti condenses as perovskite by 1600 K. But only about 40% of the total Ca has condensed by this temperature. With the formation of melilite, all remaining Ca condenses by 1500 K. Below 1400 K, pyroxene reacts to form anorthite.

With condensation calculations such as these as an underpinning, we started to study inclusions in carbonaceous chondrites like the Murchison CM2 chondrite shown in Fig. 3. The inclusions in this meteorite are only millimeters in size, so are difficult to dig out pure with standard dental tools. Consequently, we used a freeze-thaw technique to disaggregate chunks of the meteorite gently, hoping to separate the inclusions cleanly from the black phyllosilicate matrix.

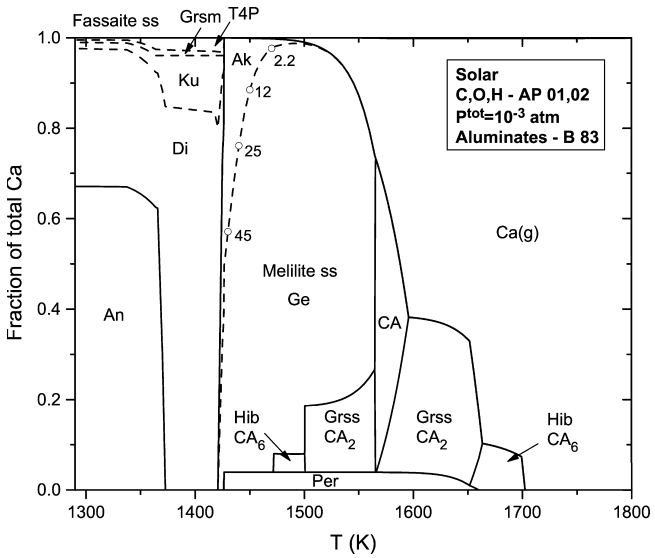

Fig. 2. Equilibrium distribution of Ca between vapor and condensed phases in a system of solar composition at a total pressure of 10^{-3} atm, calculated using the same data as in Fig. 1. Dashed curves and abbreviations as in Fig. 1, plus: Per, perovskite; Ak, åkermanite; Di, diopside. Numbers along the gehlenite-akermanite boundary curve represent mole% åkermanite in the melilite solid solution.

Fig. 3. Hand specimen of the Murchison CM2 chondrite, showing mm-sized inclusions.

Ed Olsen showed us this technique. First, we immerse the sample chip in distilled water, and evacuate the chamber so that, as air is sucked out of the pore spaces of the meteorite, water is driven in to displace it. Then we dip the container in liquid nitrogen to freeze the water (Fig. 4a). Then, we thaw the ice by warming the container to room temperature, and we repeat the entire freeze-thaw cycle (Fig. 4b). After about 20 cycles, the big chips disappear, and the ice becomes black due to

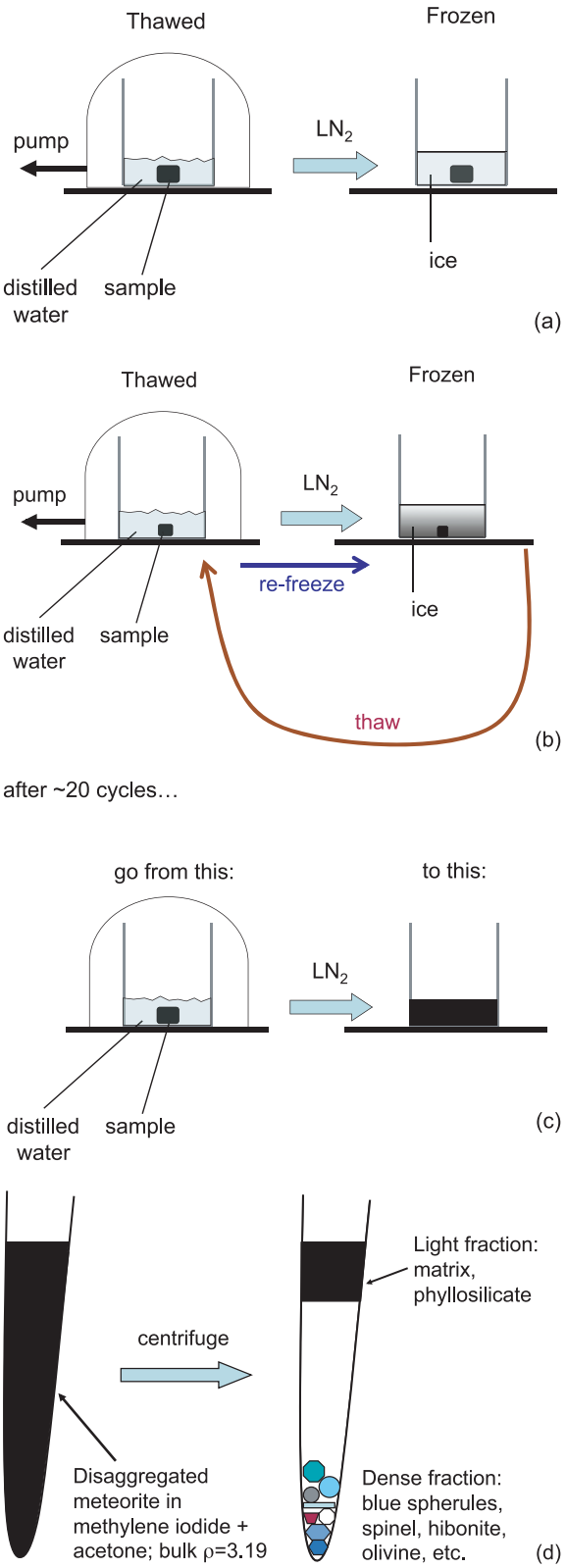

Fig. 4. a–d) Step-by-step, freeze-thaw disaggregation and density separation technique for freeing anhydrous inclusions in CM2 chondrites cleanly from their enclosing hydrous silicate matrix.

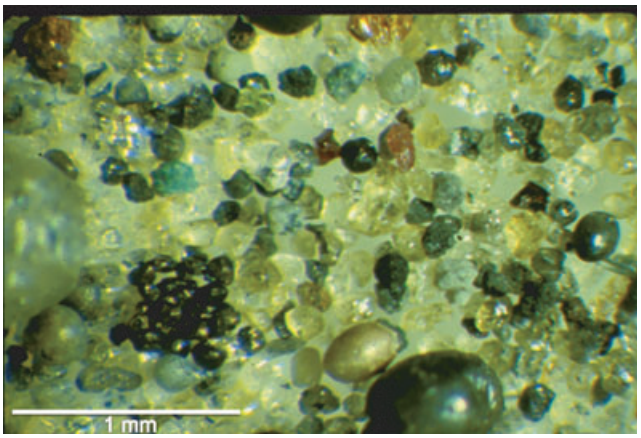

Fig. 5. Dense fraction separated from the Murchison CM2 chondrite by the technique illustrated in Fig. 4.

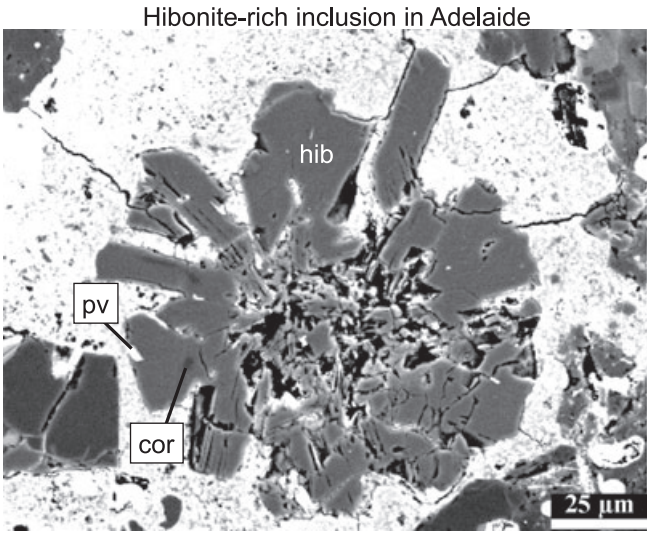

Fig. 6. Backscattered electron image (BEI) of a hibonite "snowflake" in the CM2 Adelaide, containing tiny inclusions of corundum and perovskite. Abbreviations as used previously, except pv, perovskite. Photo courtesy of A. N. Krot.

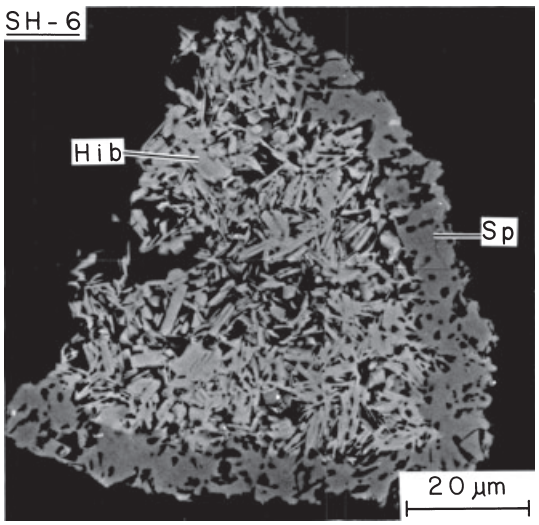

Fig. 7. Backscattered electron image of a lacy intergrowth of hibonite plates being pseudomorphically replaced by spinel. Abbreviations as used previously, plus Sp, spinel. Taken from MacPherson et al. (1984), Fig. 2a.

the particles finely dispersed within it (Fig. 4c). We thaw the ice one last time, decant the water, pour the entire solid fraction into a tube filled with an organic liquid whose density lies between those of the phyllosilicate and the anhydrous minerals of the inclusions, and then centrifuge to speed up the phase separation. As a result, the phyllosilicate floats to the top and the goodies sink to the bottom (Fig. 4d). The dense fraction actually separated from Murchison in this way by Tsuyoshi Tanaka is shown in Fig. 5. The smooth, shiny balls are chondrules, the blue inclusions contain hibonite, the red crystals are Cr-bearing spinels (Simon et al. 1994), the colorless to pale yellow crystals are very low-iron olivines, the rust-colored grains are usually pyroxenes, and the grayish, bulbous things are what we've been calling OC (for octopus) inclusions (MacPherson et al. 1983).

The refractory inclusions in CM2s and other primitive chondrites are gorgeous. This inclusion (Fig. 6) is a radiating aggregate of hibonite crystals, with a little bit of corundum and perovskite inside some of the hibonite. To me, it looks just like a snowflake. And I think it formed in the same way as a snowflake, by direct condensation from a vapor. Something with this mineralogical composition could condense from the solar nebular gas at about 1700 K at a total pressure of 10^{-3} atm, according to Figs. 1 and 2. The sample shown in Fig. 7, fished out of our Murchison density separates, is an aggregate of euhedral hibonite plates, being replaced pseudomorphically by spinel (MacPherson et al. 1984). This looks like the reaction predicted by thermodynamic calculations (Fig. 1) to occur at about 1475 K at a total pressure of 10^{-3} atm.

The CV3 carbonaceous chondrites, such as Axtell (Fig. 8) are a treasure trove of refractory inclusions. In these meteorites, the inclusions can be up to a cm in size, and so are easier to excavate with dental tools. But the refractory inclusions in these meteorites are different from those in the CM2s. Figure 9 is a backscattered electron image of what we call a Compact Type A inclusion (Simon et al. 1999). The dark, nicely-shaped crystals are spinel, the bright grains perovskite, and the background gray is melilite. According to Figs. 1 and 2, this assemblage is stable in a gas of solar composition at about 1450 K at a total pressure of 10^{-3} atm. A crossed polars view of what we call a Type B1 inclusion

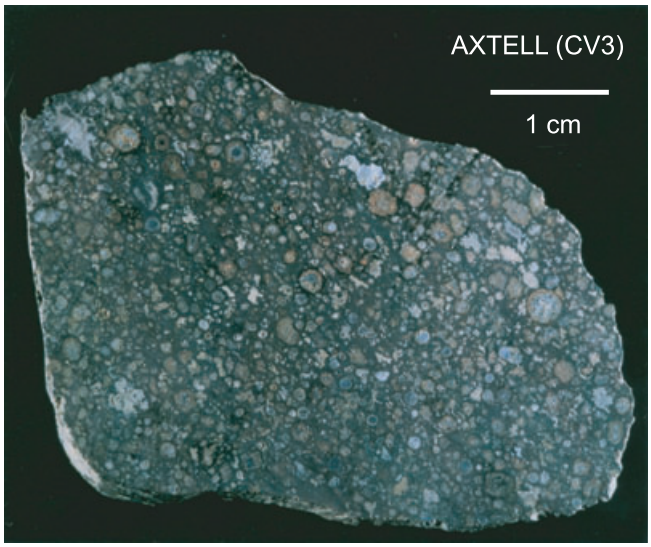

Fig. 8. Slab surface of the Axtell CV3 chondrite. Light-colored, irregularly shaped objects are refractory inclusions and amoeboid olivine aggregates. These objects reach 1 cm in diameter in these meteorites.

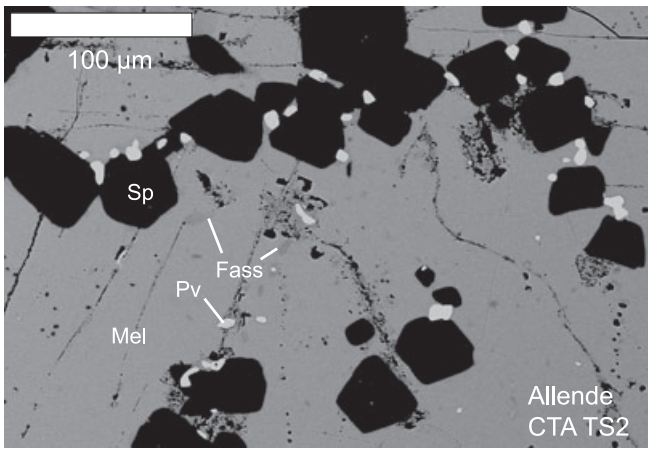

Fig. 9. Backscattered electron image of a Compact Type A (CTA) inclusion in Allende. Abbreviations as used previously, plus Fass, fassaite.

is shown in Fig. 10. Note its large size and spherical shape. Melilite is the bluish gray mineral all around the outside. Fassaite is the brightly colored stuff. And the black specks inside the fassaite are spinel. A condensate assemblage of this mineralogy could have formed at about 1425 K at a total pressure of 10^{-3} atm. So, the big difference between the refractory inclusions in CM2 chondrites and those in the CV3s is the presence of abundant silicate minerals in the latter, indicating that those in the CV3s continued to react with the gas to lower temperatures than those in the CM2s (MacPherson et al. 1984).

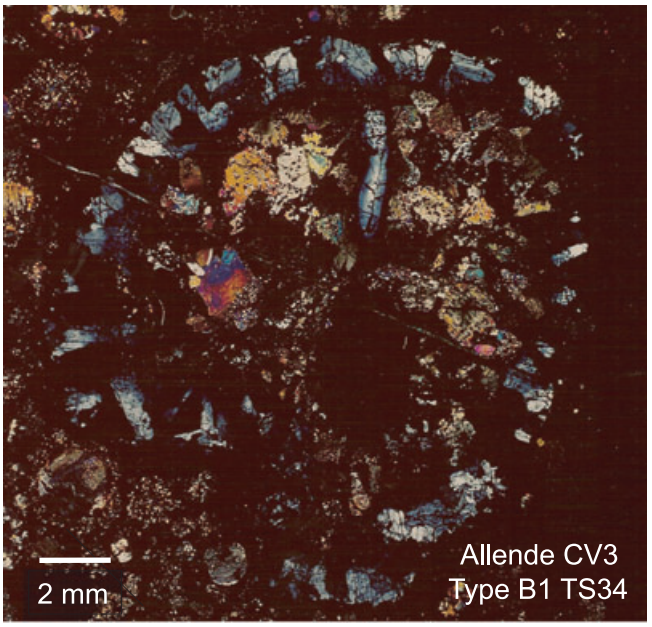

Fig. 10. Crossed polars, transmitted light view of a Type B1 inclusion from Allende. Bluish gray-melilite; brightly colored-fassaite; black specks in fassaite-spinel.

We now know that most of the Types A and B inclusions underwent melting after they condensed (Stolper and Paque 1986), but experiments such as the one by Stolper (1982), whose results are illustrated in Fig. 11, show that, when these liquid droplets cooled off, the same minerals crystallized from the liquid as those predicted to have melted to form the liquid in the first place. Spinel is the first to crystallize upon cooling, and pyroxene of fassaite composition is last, at about 1500 K.

Pyroxene in the inclusions differs from normal diopside in containing lots of Ti and Al (Mason 1974). Shown in Fig. 12 are the results of converting electron microprobe analyses of the pyroxene into numbers of cations per six oxygen anions in its chemical formula. When it is assumed that all the titanium is Ti^{4+}, note that the apparent number of cations is less than the ideal value of 4.00, and that this difference increases with increasing Ti content. This is because the valence of some of the Ti is actually $3+$. Recalculating the chemical formula to yield exactly 4.00 cations requires about half the Ti to be trivalent. This has been verified by spectroscopic techniques (Dowty and Clark 1973).

The presence of Ti^{3+} requires that refractory inclusions formed at very low oxygen fugacity; that is, where there was very little free oxygen. On Fig. 13, a graph of oxygen fugacity versus temperature, the curve along which pure metallic iron coexists stably with pure FeO, the so-called iron-wüstite buffer, is abbreviated IW. These are relatively reducing conditions. If there

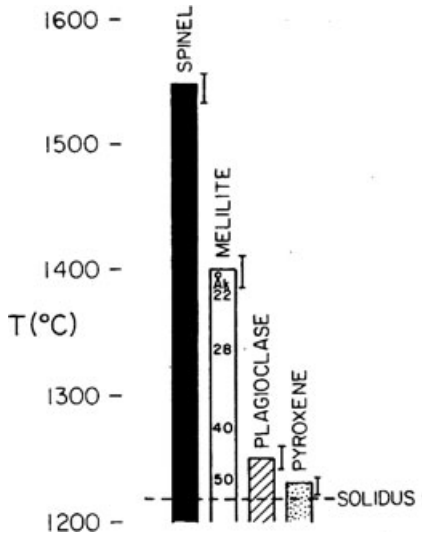

Fig. 11. Experimentally determined crystallization sequence for a representative liquid of Type B composition. When an inclusion of Type B chemical composition is melted, the equilibrium crystallization sequence upon cooling is spinel, then melilite, then anorthite, then fassaite. Adapted from Stolper (1982), Fig. 1.

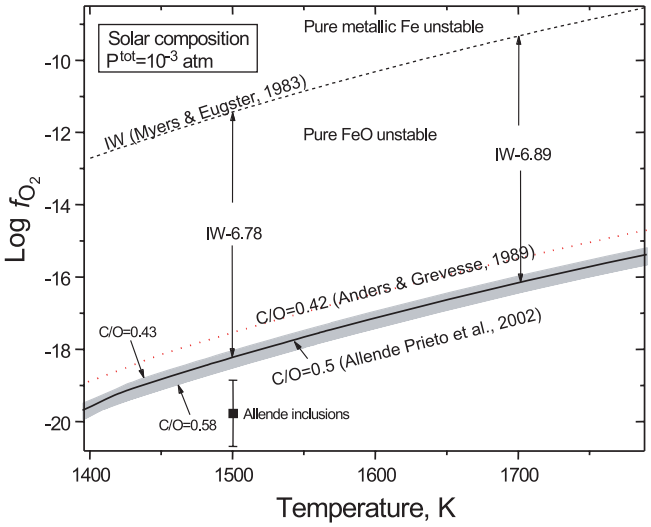

Fig. 13. Variation of the logarithm of the oxygen fugacity with temperature for the iron-wüstite (IW) buffer and for a system of solar composition. The experimentally determined value for the Allende Types A and B inclusions lies very close to the solar composition curve. Taken from Grossman et al. (2008a), Fig. 2.

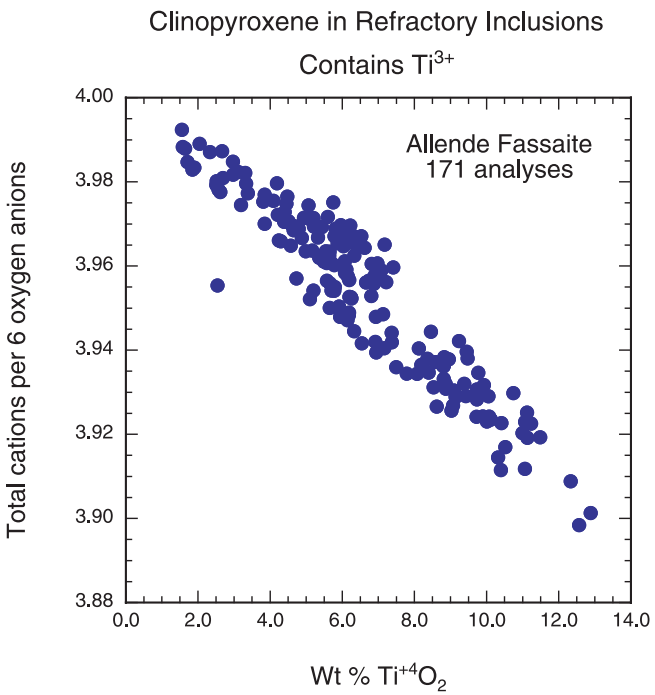

Fig. 12. Compositions of fassaite in Types A and B inclusions, plotted as total cations per six oxygen anions versus the calculated amount of titanium dioxide. When all Ti in fassaite in Types A and B inclusions is expressed as Ti^{4+}, the number of cations calculated in the chemical formula on the basis of six oxygen anions is always less than the ideal value of 4.00, and becomes smaller with increasing Ti content.

were more free oxygen than this, so-called oxidizing conditions, the metallic Fe would be converted to iron oxide, and the system would begin to approach conditions like those at the surface of the Earth. Also shown is the curve calculated for a system of solar composition, about 10 million times lower than IW due to the large amounts of H and C relative to oxygen in solar system matter. John Beckett (1986) synthesized pyroxenes with the same amount of Ti^{3+} as the pyroxene in refractory inclusions, but this required an oxygen fugacity at the pyroxene crystallization temperature that plots very close to the solar gas curve (Grossman et al. 2008a), as shown. The oxidation state of titanium in the fassaite in refractory inclusions is the only calibrated oxygen fugacity sensor that says that anything in chondrites formed in a gas as reducing as one of solar composition.

The graph in Fig. 14 shows the results of neutron activation analyses of Types A and B refractory inclusions (Grossman 1980). When the mean concentration of each of these elements in the refractory inclusions is divided by its concentration in CI chondrites, they all turn out to have the same enrichment factor relative to the total condensable matter of the solar system, approximately 17.5. While the elements shown vary considerably in chemical properties and geochemical behavior, they are all predicted to condense in the same high temperature range as the major mineral phases in the inclusions, and it is the high-temperature condensation process that has

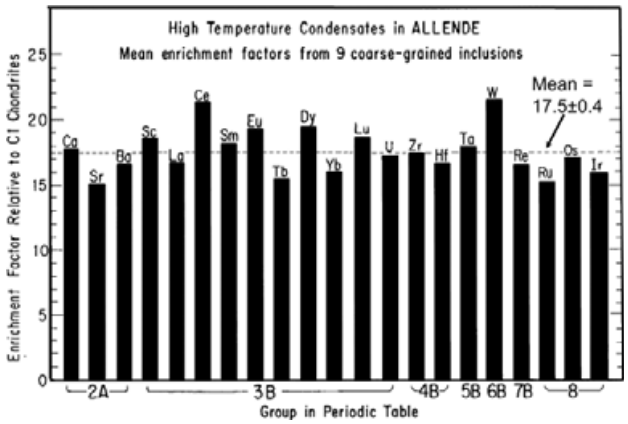

Fig. 14. Neutron activation analyses of coarse-grained, refractory inclusions from Allende. The mean concentration of each refractory element in a collection of Allende Types A and B inclusions, divided by its concentration in CI chondrites is 17.5 ± 0.4. Taken from Grossman (1980), Fig. 4.

brought all these elements together into the inclusions. Why is the enrichment factor 17.5? Suppose the concentration of a refractory element in a CI chondrite is x, and CI chondrites are representative of 100% of the Total Condensable Matter (TCM) of the solar system. Then, if all of the condensable matter were once evaporated to form a solar gas; and the entire amount of the same refractory element re-condensed into the refractory inclusions; and the inclusions represent only 5.71 wt% of the TCM, close to the value one obtains from condensation calculations as a consequence of the elemental abundances; then the concentration of the refractory element in the inclusions will be $100x/5.71 = 17.5x$, or 17.5 times its concentration in CI chondrites.

Do the inclusions represent the first 5.7 wt% of solar system matter to condense during cooling of the nebula, or the residue left after evaporation of 94.3% of condensable solar system matter? Thermodynamics can't tell the difference. It is known that the inclusions were molten while surrounded by a hydrogen-rich gas (Grossman et al. 2008a), and experiments show that Mg and Si would evaporate rapidly under these conditions (Richter et al. 2002). Furthermore, as shown in Fig. 15, the heavy isotopes of Si and Mg are enriched relative to the light isotopes in refractory inclusions (Grossman et al. 2008b), and this is a clue that these elements actually were partially evaporated from them. If it is assumed that the heavy isotope enrichments are due to kinetic isotope fractionation during evaporation of Mg and Si into a low-density gas, the Rayleigh equation can be used to convert the sizes of the isotope fractionations into the proportions of these elements evaporated from the inclusions. The results are shown in Fig. 16. Between 15 and 60% of the Mg, and 5 to 25% of the Si were evaporated from the Types A and B inclusions.

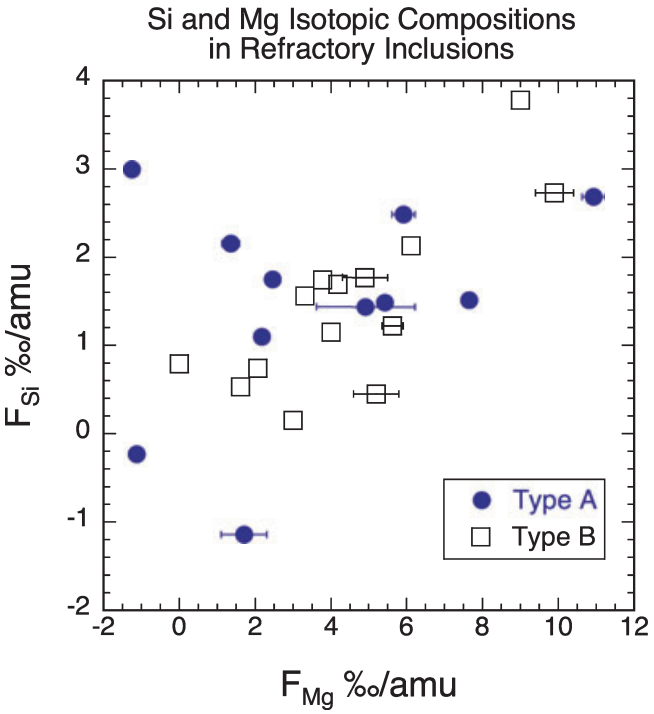

Fig. 15. Silicon and magnesium isotopic compositions of Types A and B inclusions. Types A and B inclusions are mass-fractionated toward the heavy isotopes of Mg and Si.

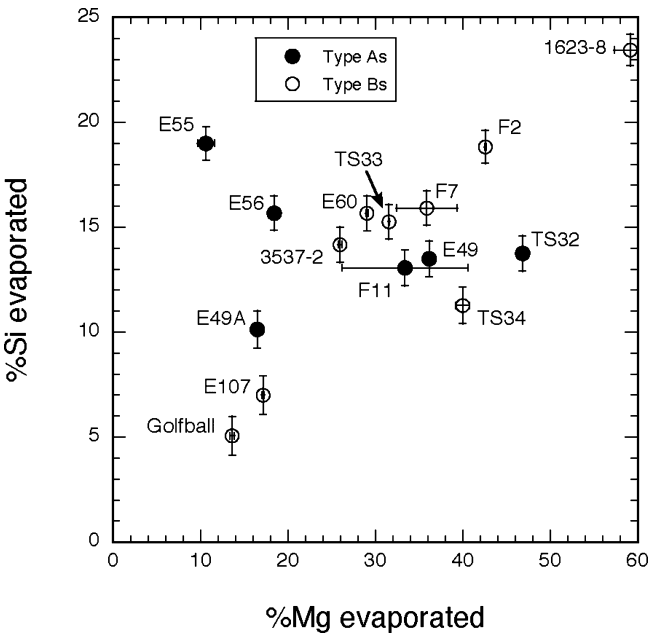

Fig. 16. Amounts of silicon and magnesium inferred to have evaporated from Types A and B inclusions. The Mg and Si isotopic fractionations can be interpreted to mean that between 15 and 60% of the Mg and between 5 and 25% of the Si were evaporated from Types A and B inclusions while they were molten. Taken from Grossman et al. (2008b), Fig. 8.

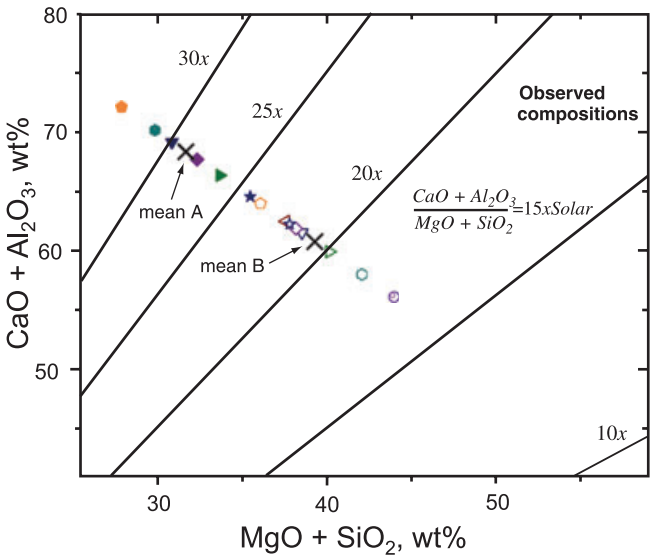

Fig. 17. The sums of the oxides of the refractory elements, Ca and Al, plotted against the sums of the oxides of the relatively volatile elements, Mg and Si, in Types A and B inclusions. It is seen that the Type As are enriched by a factor of approximately 30 and the Bs by a factor of approximately 20 in the refractories relative to the volatiles compared to solar system abundances, on average. Taken from Grossman et al. (2008b), Fig. 12a.

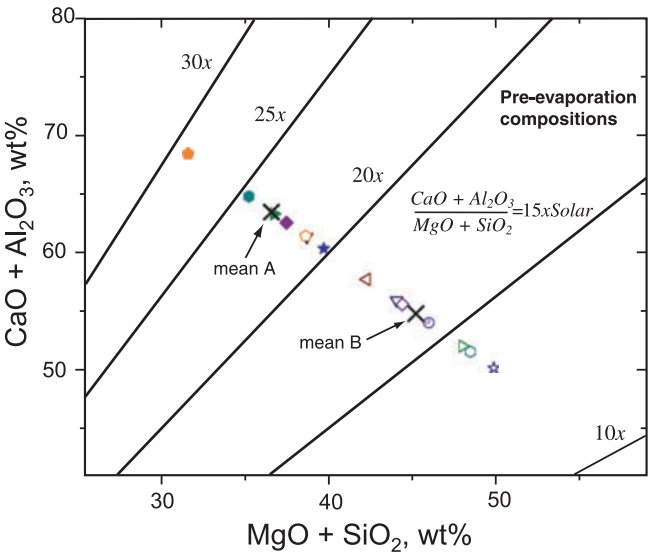

Fig. 18. Calculated compositions of refractory inclusions augmented by the amounts of Mg and Si that were lost from them by evaporation. The mean enrichment factors of refractories relative to volatiles are 24 in the Type As and 16 in the Type Bs, only 80% of their measured values, implying that 80% of the enrichment is caused by initial condensation and only 20% by subsequent evaporation. Taken from Grossman et al. (2008b), Fig. 12b.

The enrichments in refractory elements in Types A and B inclusions were shown above. The sums of the concentrations of the oxides of the refractory elements, Ca and Al, are plotted against those of the relatively volatile elements, Mg and Si, in Fig. 17. Comparison of the data points with the diagonal lines shows how much the refractories are enriched relative to the volatiles compared to the solar system abundances, about 30 times for the As and 20 times for the Bs, on average. But this relative enrichment in refractories is due to both initial condensation and subsequent evaporation of Mg and Si. When the chemical composition of each inclusion is corrected for the amounts of Mg and Si that were evaporated, and then re-plotted on the same diagram (Fig. 18), it is found that the condensation process alone caused enrichment in refractories relative to volatiles by a factor of 24 for the As and a factor of 16 for the Bs, on average. In other words, about 80% of the enrichment in refractories relative to volatiles in the refractory inclusions was caused by initial condensation; only 20% of the enrichment was caused by later evaporation.

Chondrites are not the only objects where Ca-, Al-rich refractory inclusions are found. Comets are small bodies composed of rocky and icy material whose orbits traverse both the inner solar system and its far, outer reaches. Some estimates suggest there may be as much matter in the comets as in the planets; yet, until recently, we haven't known much about their compositions. In January 2004, the Stardust spacecraft executed a close encounter with the Jupiter Family Comet Wild 2. The comet nucleus is about 4.5 km in diameter and pockmarked with impact craters. Jets of solid particles are carried outward by water vapor formed by evaporation of ice caused by solar heating, the process responsible for the beautiful cometary tails. The Stardust spacecraft was designed to capture some of these particles in low-density silica, called aerogel. Blocks of aerogel returned by the spacecraft contain tracks produced by the cometary particles as they came to rest. Hard-working teams at NASA Johnson Space Center, the Jet Propulsion Laboratory and other institutions developed ingenious ways of extracting the particles from their surrounding aerogel. Many particles have now been analyzed. They contain many of the minerals characteristic of carbonaceous chondrites. One group of particles, called Inti, found in track 25, are of particular interest to us. The minerals in the fragment of Inti seen in Fig. 19 were identified both structurally, by electron diffraction, and chemically, by energy dispersive X-ray analysis (Simon et al. 2008). Inti contains Al-rich melilite, spinel, fassaitic clinopyroxene, and anorthite, the same mineral assemblage as in the Allende Type B inclusions. This is a refractory inclusion from a comet.

In Fig. 20, the compositions of some of the pyroxene grains in Inti are compared with those in

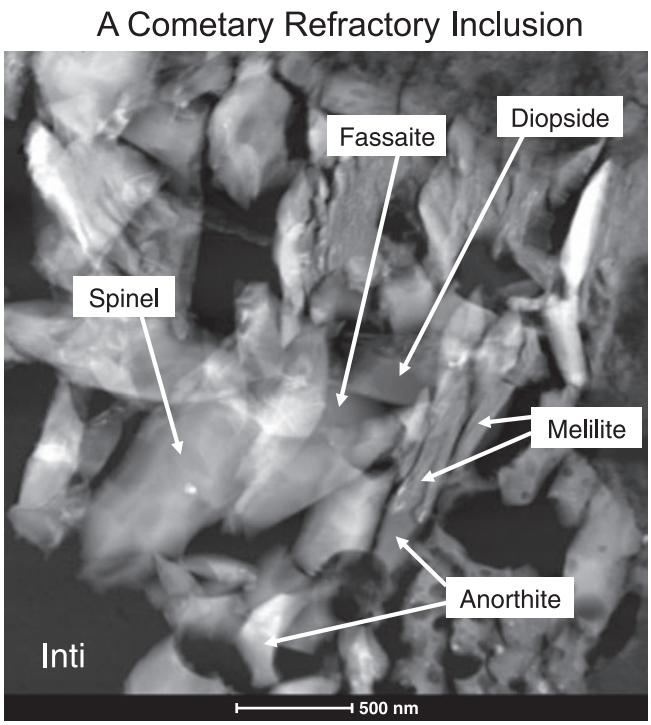

Fig. 19. High angle annular dark field image of Inti, a particle from Comet Wild 2. The mineralogical composition is the same as that of Type B inclusions. Adapted from Simon et al. (2008), Fig. 4b.

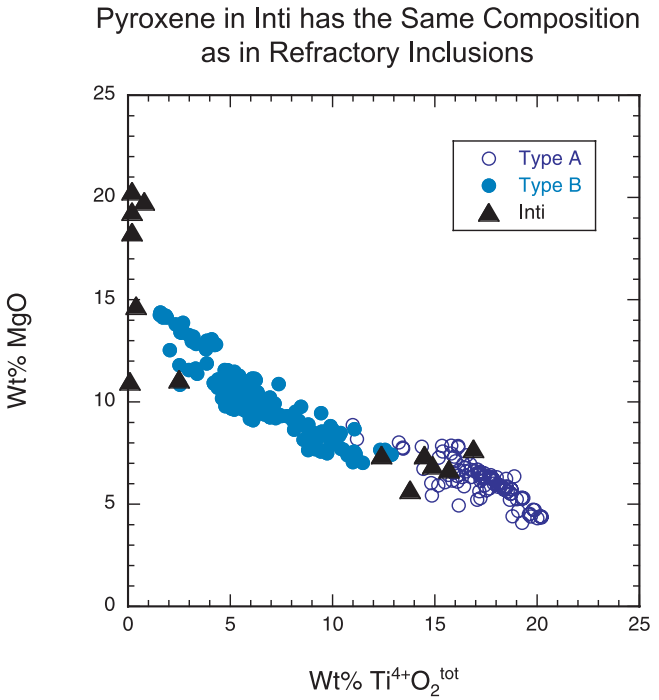

Fig. 20. Energy-dispersive analyses of pyroxene in Inti compared to wavelength-dispersive analyses of fassaite in Types A and B inclusions from Allende. The composition of some of the clinopyroxene in Inti lies along the trend for fassaite in Types A and B inclusions, implying that Inti clinopyroxene contains Ti^{3+}. Adapted from Simon et al. (2008), Fig. 8b.

Types A and B refractory inclusions in carbonaceous chondrites. Some of the Inti grains lie on the same trend as the Allende pyroxenes. In order to do so, a pyroxene must contain significant Ti^{3+}. So even the pyroxene composition in the cometary refractory inclusion is like that in Allende. Comets thus contain both refractory inclusions, the highest-temperature condensates, and ices, the lowest-temperature ones. One explanation of this incongruity is that the high-temperature condensates formed in the inner, hot part of the solar nebula and were transported, grain-by-grain, to the outer, cold part, where ices were condensing. I prefer to think that both the refractory inclusions and the ices condensed in the inner part of the solar nebula, as it cooled from over 1700 K to below 100 K.

The famous diagram from Ganapathy and Anders (1974) in Fig. 21 shows the fraction of the total condensable matter of the solar system that is actually condensed at each temperature, and which elements condense in each temperature range. So far, we have talked only about the first few percent that condensed at high temperature, labeled "refractories" here. The bulk of the condensable matter only begins to condense at a slightly lower temperature, in the form of metallic nickel-iron and pure forsterite and enstatite. The silicates are the pure magnesian end-members because

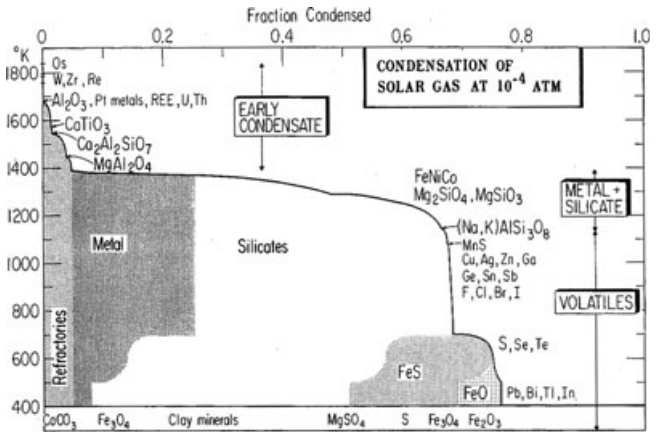

Fig. 21. The fraction of the total condensable matter calculated to have actually condensed from a solar gas as a function of temperature. Note the low temperature at which iron oxide becomes stable. Taken from Ganapathy and Anders (1974), Fig. 1.

the relatively large proportions of hydrogen and carbon compared to oxygen in solar gas make it so reducing at high temperature that only vanishingly small amounts of ferrous iron are stable. Note that oxidized iron would only become stable in a gas of solar composition at

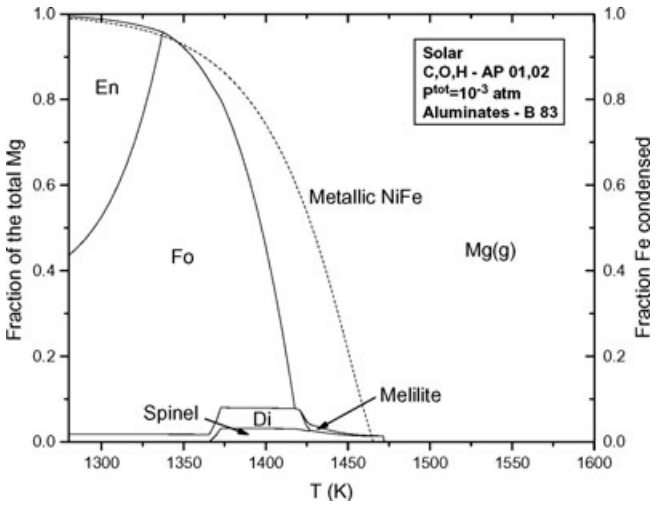

Fig. 22. Equilibrium distribution of Mg between vapor and condensed phases in a system of solar composition at a total pressure of 10^{-3} atm, calculated using the same data as in Fig. 1. Dashed curve shows the fraction of Fe condensed as an iron-nickel alloy. Abbreviations as used previously, plus: Fo, forsterite; En, enstatite.

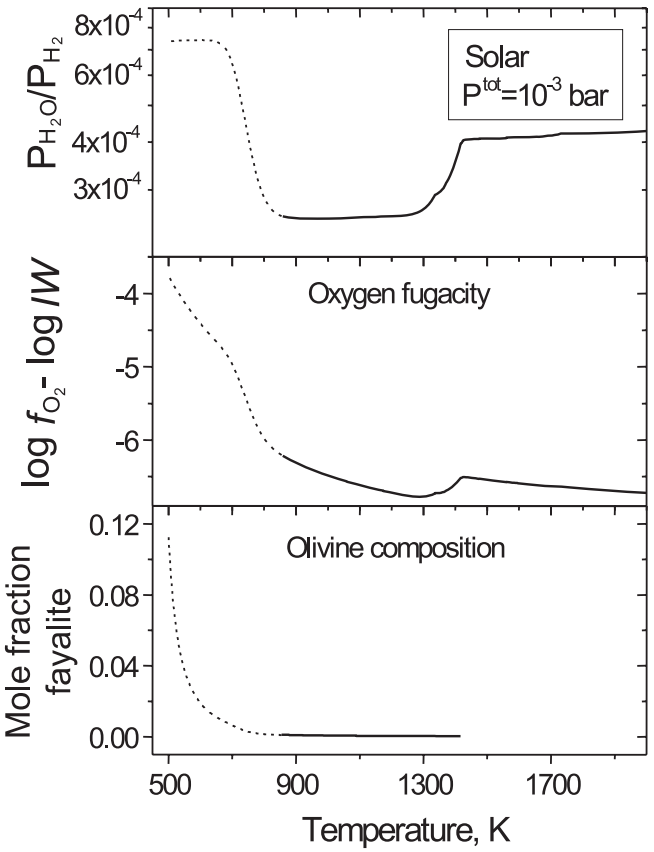

Fig. 23. The water/hydrogen ratio, logarithm of the oxygen fugacity relative to iron-wüstite and the consequent mole fraction of fayalite in olivine as a function of temperature in a system of solar composition. Dashed extensions of curves show effects of departures from gas phase equilibrium expected at low temperature. Adapted from Fedkin and Grossman (2006), Figs. 2, 3, and 4.

temperatures below 600 K. This is shown in more detail in Fig. 22. The bulk of solar system matter condenses at temperatures below where Al, Ti, and Ca have condensed. At the total pressure shown, metal condenses before forsterite, enstatite forms by reaction of forsterite with the gas, and neither silicate has any oxidized iron in it. Magnesium and Si are totally condensed as forsterite and enstatite by 1250 K.

The most important unresolved problem in applying condensation theory to the mineralogy of chondrites is understanding why the olivine and pyroxene in chondrules and matrix of carbonaceous and ordinary chondrites have such high FeO/FeO + MgO ratios, from 0.1 to 0.5 (Grossman et al. 2008a). Here's the problem. Water is the oxidizing agent in the solar nebula but, as can be seen in the upper panel of Fig. 23, its concentration doesn't build up relative to that of hydrogen until the gas temperature is below 900 K, and even then the water/hydrogen ratio is quite low, even if gas phase equilibrium could be attained. So the oxygen fugacity doesn't build up until this temperature range, and even at 500 K, it's still 4 orders of magnitude below the iron-wüstite curve, which is where pure FeO would be stable. The stable form of the oxidized iron that can exist is Fe^{2+} dissolved in olivine, and we see from the bottom panel that a significant concentration of iron could become stable in the olivine at around 500 K. But as seen above, the other constituents of olivine, Mg and Si, had already totally condensed at a much higher temperature, so no more olivine is forming in this temperature range. The only way to make the stable form of oxidized iron is by solid-state diffusion through the pre-existing olivine grains. The problem is that the Fe-Mg interdiffusion coefficient in olivine is very small at these temperatures and oxygen fugacities. In Fig. 24 is shown a calculation of how far into a one micron olivine crystal the oxidized iron can travel as the temperature falls, the oxygen fugacity builds up, the oxidized iron becomes more stable, and the diffusion rate becomes smaller. In the top panel, the nebula cools on a 1 Myr time scale; in the bottom one, in a hundred thousand years. Basically, diffusion stops at 850 K in both cases, before much oxidized iron becomes stable. The mean fayalite content of the olivine is less than a tenth of a percent. You just can't get to 10% in a solar gas.

So people have been looking for ways to make a region of the solar nebula more oxidizing than average, so that metallic iron could become oxidized at a higher temperature. One way is by dust enrichment, illustrated in Fig. 25. It's based on the idea that the bulk of the

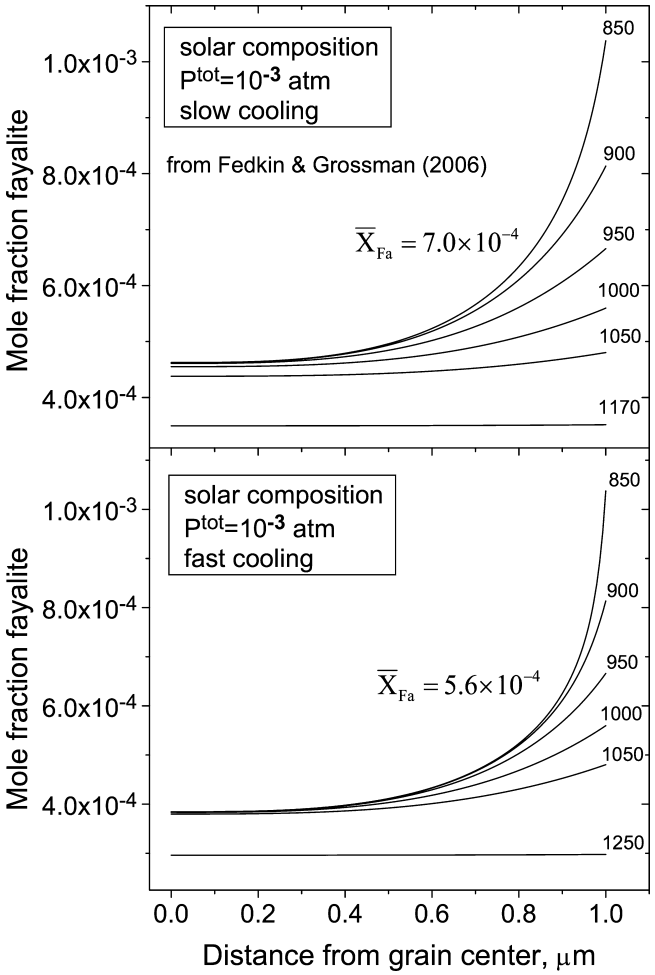

Fig. 24. Zoning profiles of fayalite in 1.0 micron-radius olivine grains calculated to have resulted from condensation in a system of solar composition at 10^{-3} atm total pressure for cooling times of 10^6 yr (a) and 10^5 yr (b). Slow Fe-Mg interdiffusion rates limit the mole fraction of fayalite in 1.0 micron-radius olivine grains to <0.001 in solar gas, far below the values observed in most chondrites, even for very long nebular cooling times. Adapted from Fedkin and Grossman (2006), Figs. 5b and 5d.

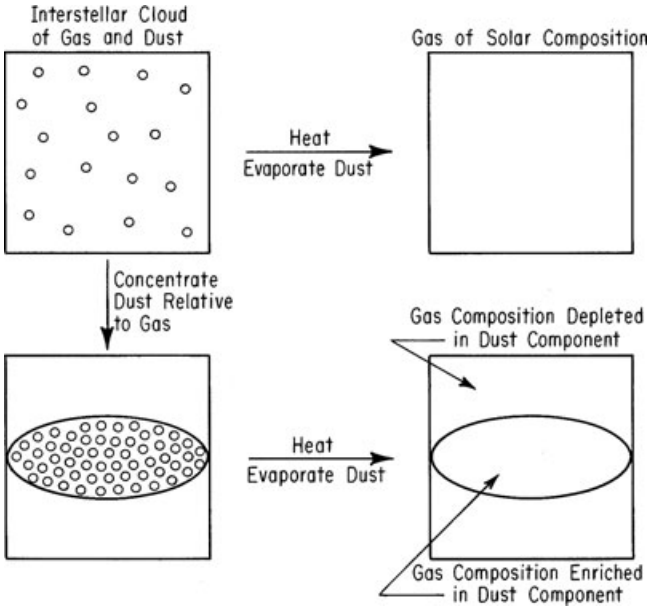

Fig. 25. Schematic illustrating how complementary mixtures of gas and dust can be heated to create either a gas of solar composition if dust is not fractionated from gas beforehand; or regions either depleted or enriched in volatilized dust relative to gas compared to solar composition, if dust is fractionated from gas.

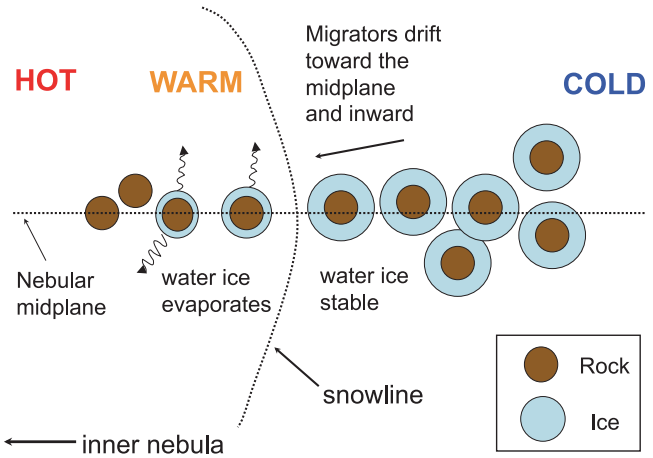

Fig. 26. Schematic illustrating enrichment of the inner part of the solar nebula in water relative to hydrogen when water-ice-containing bodies condense and accrete in the outer solar nebula, and then migrate into the inner solar nebula, where the water-ice is gradually evaporated.

condensable elements arrived in the solar nebula as interstellar dust grains. Those dust grains were totally vaporized and mixed with hydrogen and other volatiles to form solar gas. If instead, the dust were concentrated into certain regions relative to the gas before being vaporized, by gravitational settling, for example, then that region would become much more oxidizing than solar gas because the dust is enriched in oxygen compared to hydrogen and carbon. In this model, the maximum dust enrichment that can be achieved for significant-sized regions is about 120 times relative to solar abundances (Cassen 2001).

The other way is illustrated in Fig. 26. The outer reaches of the solar nebula become cold enough for condensation of water ice while the inner solar nebula is still hot. Dynamic processes cause bodies composed of ice and rock to migrate from the outer to the inner part of the solar nebula, where the ice gradually evaporates, enriching the inner part of the nebula in water compared to hydrogen, thus making it more oxidizing than a solar gas. Ciesla and Cuzzi (2006) found that the

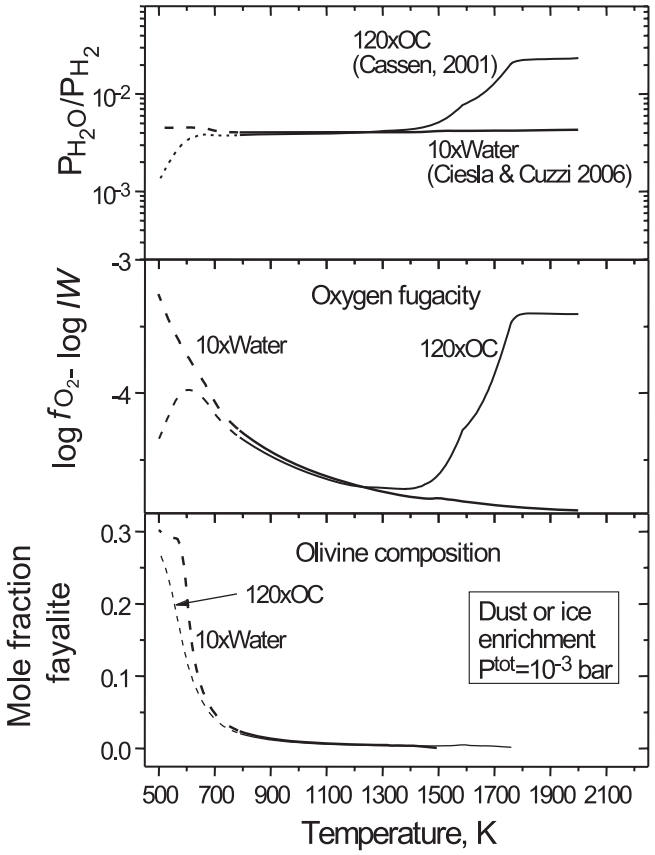

Fig. 27. The water/hydrogen ratio, logarithm of the oxygen fugacity relative to iron-wüstite and the consequent mole fraction of fayalite in olivine as a function of temperature in systems enriched 120 times in OC dust and 10 times in water relative to solar composition. Dashed extensions of curves as in Fig. 23. Adapted from Grossman et al. (2008a), Figs. 4, 5, and 6.

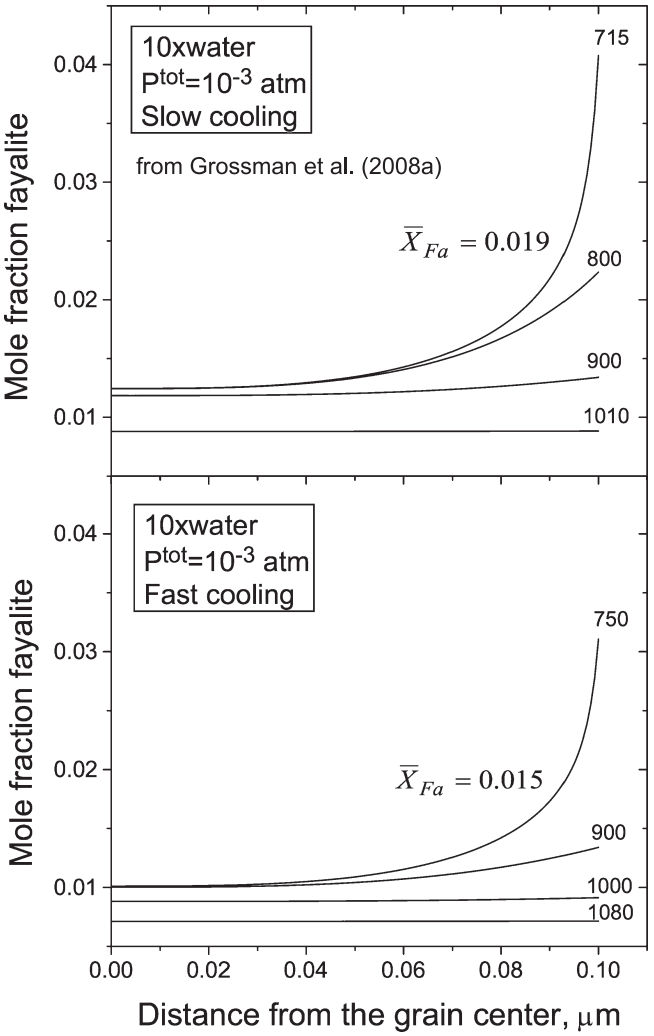

Fig. 28. Zoning profiles of fayalite in 0.1 micron-radius olivine grains calculated to have resulted from condensation in a system enriched by a factor of ten in water-ice relative to solar composition for the same conditions as in Fig. 24. Even for the case of maximum enrichment in water, 0.1 micron-radius olivine grains can reach only 2 mole% fayalite in 1 Myr. Adapted from Grossman et al. (2008a), Figs. 7b and 7d.

enrichment of water expected from this process would be no more than a factor of ten.

In Fig. 27, the effect of the maximum enrichment in dust of ordinary chondrite, or OC, composition is compared with that of the maximum ice enrichment. Below 1000 K, it is seen that the water/hydrogen ratio, the oxygen fugacity, and the resulting FeO content of the olivine are higher for the ice mechanism. If equilibrium were maintained, the olivine would reach 20% fayalite by 600 K for the ice enrichment case. But, even in these more oxidizing systems, the temperature at which the iron becomes oxidized is still too low, as shown in Fig. 28. Even for the maximum ice enrichment, an olivine grain that is only one-tenth of a micron in radius would reach only about 2% fayalite before diffusion stops for the two absurdly long cooling times mentioned previously. The mechanisms that have been proposed so far for making nebular regions more oxidizing are simply inadequate to explain the amount of oxidized iron in the silicates in most chondrites. Furthermore, the ice transport model has ignored the fact that carbon-bearing compounds will condense with and accompany the water ice on its trip to the inner nebula. If oxygen is not completely separated from carbon, the resulting system will be even less oxidizing than shown here.

CONCLUSIONS

Equilibrium thermodynamic calculations of the sequence of condensation of phases from a gas of solar composition successfully predict the mineral assemblages of refractory inclusions in CM2 and CV3 chondrites. Some of the refractory inclusions in

CM2 chondrites appear to be direct vapor-to-solid condensates that did not undergo melting or later alteration. The silica-poor refractory inclusions in CM2 chondrites were isolated from the gas at a higher temperature than the precursors of the Types A and B inclusions in CV3 chondrites. After condensation, Compact Type A and Type B inclusions were melted and resolidified while immersed in a gas of solar composition. While Types A and B inclusions were molten, they lost several tens of percent of their Mg and Si by evaporation. The degree to which Types A and B inclusions are enriched in refractories relative to volatiles is due mostly (approximately 80%) to high-temperature condensation and less so (approximately 20%) to later evaporation. No plausible way has been found to enrich a region of the solar nebula sufficiently in oxygen to explain the high concentrations of FeO in chondritic silicates.

Acknowledgments—Leonard Medal Plenary Lecture, Presented at the 72nd Annual Meeting of the Meteoritical Society, Nancy, France, July 16, 2009. I thank A. N. Krot for providing the photo of the hibonite-rich inclusion in Adelaide, A. V. Fedkin for the condensation calculations, and A. V. Fedkin and S. B. Simon for preparing figures. This work was supported by funds from the National Aeronautics and Space Administration through grant NNG05GG00G.

Editorial Handling—Dr. A. J. Timothy Jull

REFERENCES

Allende Prieto C., Lambert D. L., and Asplund M. 2001. The forbidden abundance of oxygen in the sun. *Astrophysical Journal* 556:L63–L66.

Allende Prieto C., Lambert D. L., and Asplund M. 2002. A reappraisal of the solar photospheric C/O ratio. *Astrophysical Journal* 573:L137–L140.

Anders E. and Grevesse N. 1989. Abundances of the elements: Meteoritic and solar. *Geochimica et Cosmochimica Acta* 53:197–214.

Beckett J. R. 1986. The origin of calcium-, aluminum-rich inclusions from carbonaceous chondrites: An experimental study. Ph.D. thesis. University of Chicago, Chicago, Illinois, USA.

Berman R. G. 1983. A thermodynamic model for multicomponent melts, with application to the system CaO-MgO-Al_2O_3-SiO_2. Ph.D. thesis. University of British Columbia, Vancouver, British Columbia, Canada.

Cassen P. 2001. Nebular thermal evolution and the properties of primitive planetary materials. *Meteoritics & Planetary Science* 36:671–700.

Ciesla F. J. and Cuzzi J. N. 2006. The evolution of the water distribution in a viscous protoplanetary disc. *Icarus* 181:178–204.

Dowty E. and Clark J. R. 1973. Crystal structure refinement and optical properties of a Ti^{3+} fassaite from the Allende meteorite. *American Mineralogist* 58:230–242.

Ebel D. S. and Grossman L. 2000. Condensation in dust-enriched systems. *Geochimica et Cosmochimica Acta* 64:339–366.

Fedkin A. V. and Grossman L. 2006. The fayalite content of chondritic olivine: Obstacle to understanding the condensation of rocky material. In Meteorites and the early solar system II, edited by Lauretta D. S. and McSween H. Y. Jr. Tucson, Arizona: The University of Arizona Press. pp. 279–294.

Ganapathy R. and Anders E. 1974. Bulk compositions of the moon and earth, estimated from meteorites. Proceedings, 5th Lunar Science Conference. New York: Pergamon Press. pp. 1181–1206.

Grossman L. 1972. Condensation in the primitive solar nebula. *Geochimica et Cosmochimica Acta* 36:597–619.

Grossman L. 1980. Refractory inclusions in the Allende meteorite. *Annual Review of Earth and Planetary Science* 8:559–608.

Grossman L., Beckett J. R., Fedkin A. V., Simon S. B., and Ciesla F. J. 2008a. Redox conditions in the solar nebula: Observational, experimental, and theoretical constraints. In Oxygen in the solar system, edited by MacPherson G. J., Mittlefehldt D. W., Jones J. H., and Simon S. B. Chantilly, Virginia: Mineralogical Society of America. pp. 93–140.

Grossman L., Simon S. B., Rai V. K., Thiemens M. H., Hutcheon I. D., Williams R. W., Galy A., Ding T., Fedkin A. V., Clayton R. N., and Mayeda T. K. 2008b. Primordial compositions of refractory inclusions. *Geochimica et Cosmochimica Acta* 72:3001–3021.

MacPherson G. J., Bar-Matthews M., Tanaka T., Olsen E., and Grossman L. 1983. Refractory inclusions in the Murchison meteorite. *Geochimica et Cosmochimica Acta* 47:823–839.

MacPherson G. J., Grossman L., Hashimoto A., Bar-Matthews M., and Tanaka T. 1984. Petrographic studies of refractory inclusions from the Murchison meteorite. Proceedings, 15th Lunar and Planetary Science Conference. Washington, D.C.: American Geophysical Union. pp. C299–C312.

Mason B. 1974. Aluminum-titanium-rich pyroxenes, with special reference to the Allende meteorite. *American Mineralogist* 59:1198–1202.

Myers J. and Eugster H. P. 1983. The system Fe-Si-O: Oxygen buffer calibrations to 1,500K. *Contributions to Mineralogy and Petrology* 82:75–90.

Richter F. M., Davis A. M., Ebel D. S., and Hashimoto A. 2002. Elemental and isotopic fractionation of Type B calcium-, aluminum-rich inclusions: Experiments, theoretical considerations, and constraints on their thermal evolution. *Geochimica et Cosmochimica Acta* 66:521–540.

Simon S. B., Grossman L., Podosek F. A., Zinner E., and Prombo C. A. 1994. Petrography, composition, and origin of large, chromian spinels from the Murchison meteorite. *Geochimica et Cosmochimica Acta* 58:1313–1334.

Simon S. B., Davis A. M., and Grossman L. 1999. Origin of compact type A refractory inclusions from CV3 carbonaceous chondrites. *Geochimica et Cosmochimica Acta* 63:1233–1248.

Simon S. B., Joswiak D. J., Ishii H. A., Bradley J. P., Chi M., Grossman L., Aleon J., Brownlee D. E., Fallon S., Hutcheon I. D., Matrajt G., and McKeegan K. D. 2008. A refractory inclusion returned by Stardust from Comet 81P/Wild2. *Meteoritics & Planetary Science* 43:1861–1877.

Stolper E. 1982. Crystallization sequences of Ca-Al-rich inclusions from Allende: An experimental study. *Geochimica et Cosmochimica Acta* 46:2159–2180.

Stolper E. and Paque J. M. 1986. Crystallization sequences of Ca-Al-rich inclusions from Allende: The effects of cooling rate and maximum temperature. *Geochimica et Cosmochimica Acta* 50:1785–1806.

Yoneda S. and Grossman L. 1995. Condensation of CaO-MgO-Al_2O_3-SiO_2 liquids from cosmic gases. *Geochimica et Cosmochimica Acta* 59:3413–3444.